Food Chemistry: X 14 (2022) 100296

Contents lists available at ScienceDirect

Food Chemistry: X

journal homepage: www.sciencedirect.com/journal/food-chemistry-x

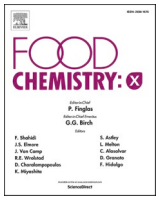

Chain conformations and steady-shear viscosity properties of pectic polysaccharides from apple and tomato

Shihao Hu [a], Junqiao Wang [b], Shaoping Nie [b], Qiang Wang [c], Xiaojuan Xu [a,*]

[a] College of Chemistry and Molecular Sciences, Wuhan University, Wuhan 430072, China
[b] State Key Laboratory of Food Science and Technology, School of Food Science and Technology, Nanchang University, Nanchang 330047, China
[c] Institute of Food Science and Technology, Chinese Academy of Agricultural Sciences, Beijing 100193, China

ARTICLE INFO

Keywords:
Pectin
Semi-rigid chain conformation
Shear thickening

ABSTRACT

In this study, apple pectin (AP) and tomato pectin (TP) were demonstrated to be a high-ester (74.8%) polysaccharide with the weight-average molecular weight (M_w) of ~ 243 kDa and a low-ester (45.9%) polysaccharide with the M_w of ~ 19 kDa, respectively. The semi-rigid chain conformations of pectic polysaccharides in $NaNO_3$ aqueous solution were deduced according to the Smidsrød "*B* values" of AP (0.025) and TP (0.029), while AP and TP exhibited higher stiffness in water due to the electric repulsion of carboxyl groups, which was visually observed by AFM images. Under steady shear, the shear-thickening behaviors of AP and TP in $NaNO_3$ aqueous solutions were observed in the shear rate range of $< 1\ s^{-1}$, which were attributed to the disruption of the ordered arrangement induced by semi-rigid pectin chains into randomly entangled structure by weak shear force. AP exhibited stronger shear-thickening behavior due to the formation of more entanglements resulted from the higher M_w and longer side chains highly branched at rhamngalacturonan region. This study provides the scientific basis for the construction of the relationship of steady-shear property with chain conformation and molecular weight of pectin.

1. Introduction

Pectin is a safe and non-toxic natural food additive recommended by the FAO/WHO Joint Committee on Food Additives (Moslemi, 2021). It is mainly used as a gelling agent in jams and jellies (Reichembach & Petkowicz, 2021), and is effective in stabilizing fruit juices and acidified milk beverages, high-protein juice beverages, and antioxidant-fortified foods (Cao, Lu, Mata, Nishinari, & Fang, 2020). Pectin also acts as a fat substitute in spreads, ice cream and emulsified meat products (Munoz-Almagro, Montilla, & Villamiel, 2021). Besides, pectin exhibits various nutritious functions such as antioxidant activity (Ma et al., 2020), intestinal protection activity (Shen et al., 2021), anti-inflammatory (Xiong et al., 2021), immunomodulatory (Zhu et al., 2021), hepatoprotective activity (Cheng et al., 2021), and inhibition of tumors (He et al., 2021), making it widely used in health food and pharmaceutical industries. The functions of pectin are largely influenced by its structure (Cui et al., 2021), and not all isolated pectins are suitable for any potential application in food or pharmaceuticals. In the future, there will be an increasing demand for high-quality pectins with specific functional and structural properties. Therefore, it is necessary to explore the structure–property/function relationship of the reproducibility and predictability of pectin.

Pectin is popularly known to be a curdled form of polysaccharide which plays a major role in ripening of fruit, making up about 30% of primary cell wall of plants (Grassino, Barba, Brncic, Lorenzo, Lucini, & Brncic, 2018). It is easily obtained because of its abundant sources such as apple (Zheng, Li, Wang, Li, Wang, & Ling, 2021), okra (Xu, Zhang, Yagoub, Yu, Ma, & Zhou, 2021), watermelon peel (Mendez, Fabra, Gomez-Mascaraque, Lopez-Rubio, & Martinez-Abad, 2021), citrus (Humerez-Flores et al., 2022), and pineapple peel (Shivamathi et al., 2022). The chemical composition and the linkages of the sugars of pectin have been widely studied. In general, pectin is mainly composed of D-galacturonic acid (D-GalA) and some neutral sugars such as rhamnose (Rha), arabinose (Ara), galactose (Gal), glucose (Glc), and xylose (Xyl) (Colodel, Vriesmann, Teofilo, & de Oliveira Petkowicz, 2018). The structure of pectin is usually divided into three regions including homogalacturonan (HG), rhamngalacturonan I (RG-I), and rhamngalacturonan II (RG-II) domains. HG is a linear chain segment composed of D-GalA residues connected by α-(1, 4)-linkages, with methoxylation at C6 and acetylation at C2 or C3. RG-I is a branched segment with a

* Corresponding author.
E-mail address: xuxj@whu.edu.cn (X. Xu).

https://doi.org/10.1016/j.fochx.2022.100296
Received 8 January 2022; Received in revised form 17 March 2022; Accepted 24 March 2022
Available online 25 March 2022

backbone of repeating disaccharide units −4)-α-D-GalA- (1, 2)-α-L-Rha-(1- and branches composed of neutral sugars linked at C4 of Rha. The length and branches of RG-I are related to the sources of pectin and extraction methods (Cui et al., 2021). RG-II is more complex and multi-branched, composed of at least 12 different monosaccharides with more than 20 different linkages (Yang, Mu, & Ma, 2018). Therefore, more efforts are needed for structural investigation of pectin.

As reported, the chemical and structural properties of pectin depend on plant species, the stage of maturity, and the method of extraction (Zdunek, Pieczywek, & Cybulska, 2021). For example, pectins extracted from creeping fig and okra by acid were low-methoxy pectins with the degree of methoxylation (DM) < 50%, while the DMs of pectins from apple (Colodel et al., 2018) and ponkan (Petkowicz, Vriesmann, & Williams, 2017) extracted by critic acid ranged from 80% to 85%. Due to the biological complexity of pectin family, the structure of pectin from different sources has to be studied individually.

The chain conformation of polysaccharides in aqueous solution plays an extremely important role in its functional properties. It was reported that the *β*-glucan from *Lentinus edodes* (Lentinan) with a triple helix conformation showed higher anti-tumor activity, while its single chains exhibited less anti-tumor activity (Surenjav, Zhang, Xu, Zhang, & Zeng, 2006). Furthermore, the higher dosage of Lentinan led to lower anti-tumor effect due to the decreased bioavailability resulting from aggregation of Lentinan (Zheng, Lu, Xu, & Zhang, 2017). Namely, the chain conformation and solution behavior such as aggregation of polysaccharides remarkably affect their functions. Therefore, it is necessary to study the chain conformation of pectin. However, there are few studies dealing with the chain conformation of pectin. Axelos and Thibauit (1991) compared the flexibility parameters *B* of pectins from different sources (apple, citrus and sugar-beet) using the method of "Smidsrød and Haug", and considered them as a relatively stiff macromolecule with rigid segments ("smooth" regions) and flexible segments ("hairy" regions), which was related to rhamnose content, degree of methylation and amidation. Morris, Torre, Ortega, Castile, Smith, and Harding (2008) characterized the "overall" conformation of pectin to be an extended or semi-flexible conformation by combination of the sedimentation conformation zoning and "Multi_HYDFIT" method, and proposed that the pectin conformation depended not only on the degree of methyl esterification but also the distribution of methyl ester groups, galacturonan content and the degree of branching by neutral sugars (e.g. galactose and arabinose). In other words, the chain conformation of pectin has diverse characteristics depending on its chemical structure. Therefore, the chain conformations of pectins from different sources are also necessary to be individually studied. Different chemical structure and chain conformation will lead to different solution properties of pectin. So far, the relationships between chain conformation and solution properties of pectin have not been fully understood.

As a rheology modifier, pectin is usually added to most products in food, medicine, personal care or household applications to achieve proper application characteristics. Like most polysaccharides, pectin exhibited a Newtonian fluid state in dilute solutions and a shear-thinning behavior in high-concentration solutions (Purnomo, Sitanggang, & Nabilah, 2021). The degree of pseudoplasticity and zero-shear viscosity were positively correlated with pectin concentration (Muhammad, Zahari, Gannasin, Adzahan, & Bakar, 2014). Interestingly, the shear-thickening behavior of a low-methoxyl pectin (DM = 35%, $M_\eta = 5 \times 10^4$) at low shear rate was also observed, which was changed to shear thinning at high shear rate (Kjøniksen, Hiorth, & Nyström, 2005). However, the mechanism of shear thickening has not been fully understood.

The pectin extracted from flesh tomato with hydrochloric acid and ammonium oxalate had low methoxy and high content of GalA (Neckebroeck et al., 2021), with the structure different from that extracted from tomato peels (Grassino, Brncic, Vikic-Topic, Roca, Dent, & Brncic, 2016a; Zhang, Xie, Liu, Luo, Wu, & Wang, 2019), and the characterization of its detailed structure was still not fully understood. Meanwhile, due to the biological complexity of pectin family, it is impossible to fully understand the structure and function of all pectin families. Therefore, such an effort should be undertaken for apple at least as it is the major source of pectin (Barreira, Arraibi, & Ferreira, 2019). In this study, we thus chose two representative pectins from apple and tomato, which were widely derived and structurally different, to study there chemical structure as well as the chain conformation. And our research aims to clarify the correlation of steady-shear viscosity properties in solutions to their primary structure and chain conformation, which will help to improve our understanding of the properties of pectin and tailor new functions in food industry based on natural but often biologically variable sources.

2. Materials and methods

2.1. Materials and chemicals

The ripe apples (Red Fuji) and tomatoes (Iseaei tomato) produced in Shandong province of China were used in this work, which were purchased from the supermarket. Ethanol, acetone, citric acid, oxalic acid, ammonium oxalate, dimethyl sulfoxide (DMSO), Carbazole ($C_{12}H_9N$), sodium nitrate ($NaNO_3$), acetic anhydride ($(CH_3CO)_2O$) and sodium azide were of analytical grade, while methanol and chloroform were of high-phase liquid chromatography grade (Sinopharm Chemical Reagent Co., Ltd., Beijing, China). All the chemicals were purchased from Shen Test Chemical Co., Ltd. (Wuhan, China). The sugar standards including Glc, fucose (Fuc), Ara, Xyl, Gal, GalA, Rha, and mannose (Man) were purchased from Sinopharm Chemical Reagent Co., Ltd. (Beijing, China). Methyl iodide (CH_3I) was purchased from Energy Chemical Reagent Co., Ltd. (Shanghai, China). Sodium borodeuteride ($NaBD_4$), N-(3-Dimethylamino-propyl)-N′-ethyl-carbodiimide hydrochloride (EDC), and trifluoroacetic acid (TFA) were purchased from Sigma-Aldrich Co. Ltd. (St. Louis, Missouri, USA). 1-Phenyl-3-methyl-5-pyrazolone (PMP) was purchased from Aladdin Co., Ltd. (Shanghai, China).

2.2. Preparation of pectins

Apple pectin (AP) and tomato pectin (TP) were prepared according to the reported procedures (Grassino, Halambek, Djaković, Brnčić, Dent, & Grabarić, 2016b; Kermani et al., 2014), as described in Fig. S1. Briefly, the apples and tomatoes were cut into pieces after removing the peel, which were boiled for 10 min to inactivate enzymes; after cooling, the heat-treated residues were squeezed by a juicer, followed by decolorizing with ethanol (for apple) or acetone (for tomato) for five times. The left pomace was collected and dried in an oven with air circulation at 50 °C. Apple pomace was dipped into 20 mg/mL citric acid solution (pH 2.2) with the solid–liquid ratio of 1:50 (weight/volum, g/mL) at 85 °C for 1.5 h, and tomato pomace was soaked in 20 mg/mL ammonium oxalate-oxalic acid solution (4:1, pH 3.8) with the solid–liquid ratio of 1:40 (weight/volum, g/mL) at 90 °C for 24 h. The solutions were collected by centrifugation (10000 *g*, 15 min), followed by adding an equal volume of ethanol for precipitation and standing overnight. The precipitates were washed with 75% (v/v) ethanol/water mixture and redissolved in water, followed by dialyzing in pure water and freeze-drying to get the resulting pectin samples of AP and TP with white color.

The yield of pectin was determined according to the following formula.

$$\text{Yield } (\%) = \frac{\text{mass of dried pectin } (g)}{\text{mass of dried crude pomace } (g)} \times 100 \ \% \quad (1)$$

The ash content of pectin samples was measured by a thermogravimetric analyzer (TGAQ500, TA Co. Ltd., USA) after drying overnight at 60 °C. The initial temperature of the experiment was 30 °C, which was then raised to 600 °C at a rate of 10 °C/min. The ash content (%) was determined according to the following formula.

$$\text{Ash}\ (\%) = \frac{m_1\text{-}m_2}{m_3\text{-}m_2} \times 100\% \quad (2)$$

where m_1 is the total mass of the crucible and ash, m_2 is the mass of crucible, and m_3 is the total mass of crucible and pectin.

The protein content of pectin samples was estimated by Kjeldahl Method, and the nitrogen content was detected by VARIO EL III (Elementar Co. Ltd., Germany) elemental analyzer.

2.3. Monosaccharide composition analysis

The monosaccharide compositions of pectin samples were analyzed using a high-performance liquid chromatography (HPLC) system equipped with a PDA 2996 detector (Waters 2695, Waters Co. Ltd., USA) according to the reported methods (Zhi et al., 2017). In brief, AP and TP were hydrolyzed in 2 M TFA at 120 °C for 6 h. Subsequently, the TFA was removed by rotational evaporation under reduced pressure at 50 °C, followed by washing with methanol for several times to achieve the neutralization. The standard sugar samples were prepared by equimolarly mixing Glc, Fuc, Ara, Xyl, Gal, GalA, Rha, and Man. The hydrolyzed samples or standard sugar samples were dissolved in 450 μL of 0.3 M NaOH aqueous solution, which were used for derivatization with 450 μL of 0.5 M PMP/methanol solution at 70 °C in the dark for 30 min, followed by neutralization with 450 μL of 0.3 M HCl. Unreacted PMP was removed with chloroform, and the aqueous layer was used for HPLC analysis after filtration through a 0.22 μm membrane filter.

A Zorbax Aclips XDB-C18 column (4.6 mm × 250 mm, 5 μm, Agilent Co. Ltd., USA) was used at 35 °C. A linear gradient elution of buffer A (0.1 M sodium phosphate with pH 6.9) and buffer B (acetonitrile) was applied with the gradient of 83%-17% for 20 min. The flow rate of 0.8 mL/min was used, and the detection wavelength was 250 nm at which PMP-labeled sugars showed strong UV absorbance.

2.4. Fourier transform infrared (FT-IR) spectroscopy

The pectin samples (2 mg) were placed in a vacuum desiccator at 40 °C for 24 h to remove moisture before use. The dried samples were mixed, ground, and pressed into tablets with potassium bromide (KBr) in a macro sampling cup, which were used for structural analysis performed on a FT-IR Spectroscopy analyzer (NICOLET 5700 FTIR Spectrometer, Thermo Co. Ltd., USA) with a resolution of 4 cm^{-1} from 64 scans at the wavenumber range of 4000–400 cm^{-1}. The spectra and baselines were calibrated using the built-in software (Ominic 7.2) of the spectrophotometer.

2.5. Degree of methoxylation (DM)

The DMs of pectin samples were estimated by determining the proportion of methyl esters in conjunction with the total uronic acid content according to the reported method (Voragen, Schols, & Pilnik, 1986). Pectin samples were mixed with 50% (v/v) isopropanol/0.4 M NaOH to remove ester groups at room temperature for 120 min, followed by centrifugation at 2000 × *g* for 10 min to collect the supernatant used for gas chromatography (GC 6890, Agilent Co. Ltd., USA) measurement. The area normalization method was used for quantitative analysis of methanol content, and the DM was calculated as moles of methanol per 100 mol of GalA (corrected by galacturonic acid content).

2.6. Hydrogen nuclear magnetic resonance (^{1}H NMR) spectroscopy

The ^{1}H NMR measurement of AP and TP was performed on an NMR instrument (Bruker AVIII 400 M, Bruker Co. Ltd., Switzerland). To avoid the interference of hydrogens (H) of hydroxyls, hydrogen protons of hydroxyls in the pectin samples were exchanged with deuterium (D) by dissolving in deuterated water (D_2O, 99.9%) and vacuum-freeze drying, which was performed for 3 cycles to completely exchange H with D before analysis. The deuterated pectin samples were dissolved in D_2O with a concentration of 35 mg/mL (AP) and 50 mg/mL (TP), followed by recording the ^{1}H NMR spectra according to the standard Bruker procedures at 35 °C with sodium trimethylsilyl propionate (TSP) as the internal standard.

2.7. Methylation analysis

β-Condensation usually occurs during the repeated methylation process due to the existence of esterified GalA. Moreover, acidic polysaccharides are extremely difficult to be dissolved in DMSO. Firstly, the carboxyl groups (COOH) of pectin were reduced according to the reported EDC-$NaBD_4$ method (Taylor & Conrad, 1972) before methylation. Herein, $NaBD_4$ was used for distinguishing GalA and Gal after decarboxylation.

The reduced AP and TP were then permethylated according to the reported procedures (Ciucanu & Kerek, 1984). Afterwards the permethylated samples were depolymerized with 90% formic acid at 100 °C for 4 h and further hydrolyzed with 2 M TFA at 120 °C for 6 h. The methylated monosaccharides were reduced by $NaBD_4$ and acetylated by acetic anhydride, and the resulting permethylated alditol acetates (PMAAs) were analyzed using gas chromatography (GC)-mass spectrometry (MS) (450 GC-320 MS, Varian Co., Ltd., USA). The initial column temperature was maintained at 100 °C for 5 min, which was then raised to 250 °C at 10 °C/min and maintained for 20 min.

2.8. Intrinsic viscosity measurement

Intrinsic viscosity ([η]) measurement of pectin samples in aqueous solution was carried out on a Ubbelohde capillary viscometer at 25 ± 0.01 °C. Pectin samples were dissolved in water containing various $NaNO_3$ concentrations from 0 to 0.1 M. The [η] values were determined according to Huggins (4) and Kraemer (5) equations.

$$\frac{\eta_{sp}}{c} = [\eta] + k'\ [\eta]^2 c \quad (4)$$

$$\frac{\ln\eta_r}{c} = [\eta] - k''[\eta]^2 c \quad (5)$$

where η_r is the relative viscosity, η_{sp} is the specific viscosity, c is the pectin concentration (mg/dL), k' is characteristic of a given solute–solvent system, which is the same for solutions of a polymer-homologous series in a given solvent, and k'' is a constant dependent on the polymer and solvent (Kraemer's constant) (Huggins, 1942). The linear functions were extrapolated to the concentration of zero for obtaining the [η] value at the intercept.

2.9. Molar weight and size distribution measurement

Molar mass and size distribution of the pectin samples were analyzed using size-exclusion chromatography combined with multi-angle laser light scattering (SEC-MALLS) equipped with a He − Ne laser at $\lambda = 633$ nm (DAWNDSP, Wyatt Technology Co. Ltd., CA, USA) according to literature with some modifications (Wei et al., 2019). The pectin samples were dissolved in 0.25 M $NaNO_3$ solution with a concentration of 1 mg/mL, which were made optically clean by filtration through 0.22 μm filters before measurement. Detection was performed at 30 °C by injecting 0.5 mL samples into the columns of Shodex OHpak SB-806 HQ and SB-804 HQ (Showa Denko Co. Ltd., Tokyo, Japan) (8 × 300 mm^2) with 0.25 M $NaNO_3$ containing 0.02 % Proclin 300 (bacteriostatic agent) as eluent at a flow of 0.5 mL/min. The refractive index increment (dn/dc) values were determined to be 0.136 mL/g for AP and 0.141 mL/g for TP in 0.25 M $NaNO_3$ aqueous solution on a differential refractive index detector at λ = 633 nm (DAWN DSP, Wyatt Technology) and 30 °C (Fig. S2). The excess reduced scattering intensities R_θ obtained as a function of scattering angle θ and polymer mass concentration c were

analyzed by using of the plots of (Kc/R_θ) vs k^2. Here, K is the optical constant, and k is the magnitude of the scattering vector defined by $k = (4\pi n/\lambda)\sin(\theta/2)$, with n being the solvent refractive index. The weight-average molecular weight (M_w), number-average molecular weight (M_n), polydispersity index d (M_w/M_n), and z-average radius of gyration (R_z) were analyzed using ASTRA 6.0 software (Wyatt Technology).

2.10. Atom force microscopy (AFM)

Molecular chain morphologies of AP and TP dissolved in water were observed on a PicoScan 2500 PicoSPM II Controller (Cypher-ES, OXFORD Co. Ltd., US). The commercial MAC lever TT tips with a spring constant of 1.7 N/m were used. 5 μL of pectin dissolved in pure water (1 μg/mL) was cast on the freshly cleaved mica and dried overnight before observation. Tapping mode was conducted in air using a nanoscope system operated under ambient conditions with standard silicon tips. The height and length of pectin chains were analyzed with an Ipwin image processing software.

2.11. Scanning electron microscope (SEM)

Morphological analysis of AP and TP samples was performed on a field emission SEM (Verios460, FEI Co. Ltd., USA). The pectin samples dissolved in water with different concentrations (1.0 mg/mL, 0.1 mg/mL, and 0.01 mg/mL) were quickly dipped into liquid nitrogen for quick refrigeration, followed by lyophilization to get the dry pectin samples. They were then subjected to gold coating at a current intensity of 20 mA for 30 s and observed at an accelerating potential of 10 kV.

2.12. Steady-shear viscosity measurement

Pectin samples were dissolved in water (20 mg/mL) with different $NaNO_3$ concentrations from 0 to 0.1 M. Additionally, pectin samples were dissolved in pure water or 4 M urea with different concentrations from 5 mg/mL to 30 mg/mL. Steady-shear rheology test was performed on an ARES-RFS III rheometer (TA Co. Ltd., New Castle, USA) using a cone plate mold (diameter 60 mm, angle 0.5069°) or concentric cylinder mold (Mold length $L = 33$ mm, outer cylinder diameter $R_1 = 34$ mm, inner core diameter $R_2 = 32$ mm). The temperature was controlled at 25 ± 0.1 °C, and the shear rate was used in the range of 0.01 s^{-1} ~ 500 s^{-1}. The apparent viscosity-shear rate data of pectin was fitted with a power law model (Equation 6) (Purnomo et al., 2021),

$$\eta_a = k\dot{\gamma}^{n-1} \quad (6)$$

where η_a is apparent viscosity (Pa.s), k is consistency index, $\dot{\gamma}$ is the shear rate (s^{-1}), and n is the flow behavior index.

2.13. Statistical analysis

All the data were expressed as the mean ± standard deviation (SD), which were assessed by a one-way analysis of ANOVA to demonstrate differences between groups.

3. Results and discussion

3.1. Chemical composition and linkage analysis

The chemical and structural properties of pectin depend on at least three main factors: plant species, maturity/biological stage, and extraction method (Zdunek et al., 2021). As shown in Table 1, the yields of AP and TP polysaccharides were relatively low (~11%) compared with other reports. Ziari, Ashtiani, and Mohtashamy (2010) reported that the yield of AP ranged from 10.1% to 15.2% depending on extraction time, temperature and pH. Sengar, Rawson, Muthiah, and Kalakandan (2020) reported the pectin yield of fresh tomato to be 9.3% ~25.4% due to different extraction techniques. The low yields of AP and TP in this study might be resulted from purification by alcohol fractional precipitation for removing some small molecular polysaccharides, and was also related to the origin, ripe state and extraction method of the fruit (Marić et al., 2018). Ash and protein content was determined to be below 5%, indicating the relatively high purity of pectic polysaccharides. The basic structural characteristics including degree of methoxylation, sugar composition and glycosidic linkages of sugars were analyzed in the following, respectively.

Table 1
Yield and component analysis results of AP and TP. The superscripts of a and b mean significant differences at $p < 0.01$.

Items	AP	TP
Yield (%)	11.2	11.1
Ash (%)	4.8 ± 0.3	2.3 ± 0.4
Protein (%)	3.6 ± 0.1	4.9 ± 0.2
DM (%)	74.8 ± 0.3	45.9 ± 0.2
Monosaccharides (mol %)		
Rha (%)	3.9 ± 0.3[a]	7.8 ± 1.0[b]
Glc (%)	0.9 ± 0.2	0.8 ± 0.2
Gal (%)	7.0 ± 0.6	10.7 ± 0.7
Xyl + Ara (%)	40.0 ± 1.5[a]	9.7 ± 2.1[b]
Fuc (%)	0.3 ± 0.04	ND
GalA (%)	47.8 ± 2.2[a]	71.0 ± 1.5[b]
HG	43.9	63.2
Rha/GalA	0.08	0.1
(Gal + Ara + Xyl)/Rha	12.1[a]	2.6[b]
GalA/(Fuc + Rha + Ara + Gal + Xyl + Glc)	0.9[a]	2.5[b]

Note:
HG was obtained by subtracting the content of Rha from the total GalA content.
Rha/GalA, the contribution of RG to pectic population;
(Gal + Ara + Xyl)/Rha, the length of side chains attached to RG;
GalA/(Fuc + Rha + Ara + Gal + Xyl), the linearity of pectin.

3.1.1. FT-IR and DM of pectin

The FT-IR spectra of the pectin samples are shown in Fig. 1. Some typical characteristic peaks of AP and TP were identified. The strong and broad peak appeared in the wavenumber of 3600 ~ 3000 cm^{-1}, which was attributed to the stretching vibration of hydroxyl group (OH) in polysaccharides. The peak at 2938 cm^{-1} was assigned to C—H stretching vibration from $-CH_2$ groups in the sugar ring (Tang et al., 2021). The bands at about 1745 cm^{-1} and 1610 cm^{-1} were respectively assigned to the stretching of C═O (esterified carbonyl) and COO^- (free carboxyl groups), which was used for rough quantification of DM from the ratio of

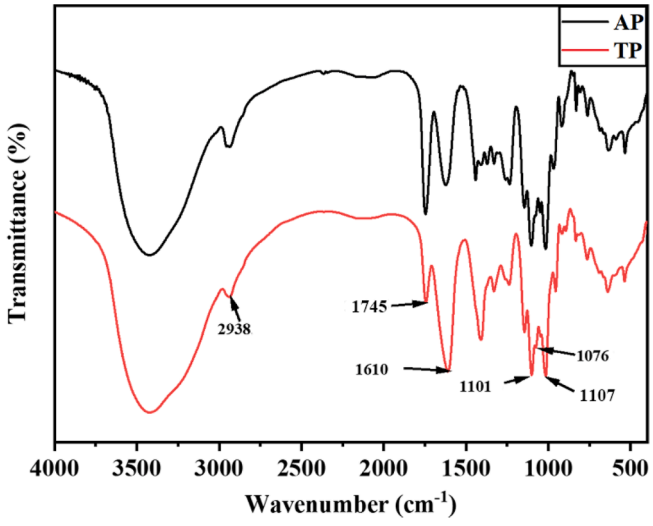

Fig. 1. FT-IR spectra of AP and TP.

the peak area at 1745 cm^{-1} to the sum of the peak areas of 1745 cm^{-1} and 1610 cm^{-1} (Kyomugasho, Christiaens, Shpigelman, Van Loey, & Hendrickx, 2015). The DMs of AP and TP were thus estimated to be 68.0% and 44.3%, indicating that AP was a high-methoxy pectin and TP was a high-methoxy pectin. To further confirm this result, AP and TP were de-esterificated, and the content of methanol was detected for determination of DM. As a result, the DMs of AP and TP were estimated to be 74.8% and 45.9%, respectively (Table 1, Fig. S3), in agreement with the results from FT-IR.

The range of 800–1300 cm^{-1} is often referred to the fingerprint region of pectin, in which the adsorption bands at 1101 cm^{-1} and 1017 cm^{-1} were resulted from stretching vibrations of glycosidic bonds (C—O) and pyranoid rings (C—C) (Zhang et al., 2019). It was worth noting that, unlike the potato pectin, very weak absorption peaks at 1076 cm^{-1} for AP and TP were attributed to the effect of acetyl group on sugar rings (Yang et al., 2018), indicating that the degrees of acetylation (DAs) of AP and TP were extremely low. From the above analysis, AP was identified as a highly methoxylated pectin (HMP) with a DM of 74.8% more than 50%, and TP was a lowly methoxylated pectin (LMP) with a DM of 45.9%. The DM of TP extracted from fresh tomatoes was close to that of pectin (54.3%) extracted from tomatoes (Solanum lycopersicum var. San Marzano) by Neckebroeck et al. (2021), but lower than that of pectin (76.0%-87.9%) from tomato peels (Grassino et al., 2016a; Grassino et al., 2016b; Sengar et al., 2020), which was ascribed to the different species and extraction methods.

The DM of pectin plays a decisive factor in determining the characteristics of physical gel. As reported, the HMP easily formed a physical gel in the presence of sufficient soluble solids (such as sucrose) at low pH, while the divalent cation as a bridge was necessary for physical gel formation of LMP (Celus, Kyomugasho, Van Loey, Grauwet, & Hendrickx, 2018). It could be expected that AP and TP with different DMs exhibited different solution behaviors.

3.1.2. Sugar compositions of pectin

The monosaccharide composition indirectly reflects the structure of polysaccharides. As shown in Table 1 and Fig. S4, AP and TP were composed of similar monosaccharide types, including sugars of Rha, Glc, Gal, GalA, Ara, and Xyl. Fuc was not detected in TP, but marginally existed in AP. The GalA was the major monosaccharide in both AP and TP. It was worth noting that the molar ratios of monosaccharides in the two pectic polysaccharides were quite different. The content of GalA, Rha, and Gal in AP was less than that in TP; while the content of other neutral sugars such as Glc, Xyl and Ara in AP was higher than those of TP. The content of Ara in AP was higher than that of pectin extracted from Golden Delicious apples (Pieczywek, Kozioł, Płaziński, Cybulska, and Zdunek, 2020). According to the previous report that the equimolar GalA was linked with Rha in RG domains (Dranca & Oroian, 2018), the HG region could be estimated by subtracting the content of Rha from the total GalA content. AP was thus found to contain 43.9% HG and TP had 63.2% HG, suggesting that TP was smoother than AP due to the predominance of HG region in TP.

The molar ratio of Rha/GalA reflected the relative abundance of the contribution of RG to pectin, the higher value of which corresponded to the higher proportion of RG region (Yang et al., 2018). As shown in Table 1, TP had a little higher ratio of Rha/GalA (0.11) than that of AP (0.08), indicating that TP had slightly longer RG region than AP. AP showed a much higher of (Ara + Xyl + Gal)/Rha value (12.1) than TP (2.6), suggesting that the length of side chains linked to RG domain of AP was much longer than that of TP or AP had more side chains highly branched in RG region (Zhi et al., 2017). The ratio of GalA/(Fuc + Rha + Ara + Gal + Xyl + Glc) for TP (2.5) was more than twice that of AP (0.9), indicating that the HG domain of TP had a stronger linearity than AP (Wang et al., 2016). In short, AP had a relatively shorter HG region and much longer side chains linked to RG region; while TP had a relatively longer HG and much shorter side chains of RG domains.

To get more structural information of AP and TP samples, the ^1H NMR spectra were obtained and shown in Fig. 2. A very intense signal at ~ 3.80 ppm was assigned to methoxyl groups (OCH_3) binding to carbonyl groups (C═O) of GalA (Liu et al., 2018). Moreover, the hydrogen signal of OCH_3 in AP was much stronger than that in TP, suggesting AP had higher methyl ester content than TP. These data were consistent with the major content of GalA in Table 1 and the DM data estimated from FT-IR and GC. The major proton signals of GalA in both AP and TP were assigned as follows: H-1, 5.09 ppm; H-2, 3.74 ppm; H-3, 4.00 ppm; H-4, 4.13 ppm and H-5, 4.44 ppm according to the reported pectin (Tang et al., 2021). Besides, in the anomeric region, partial proton signals of Ara (H-1, 5.19 ppm; H-5, 3.96 ppm) and Rha (H-1, 5.15 ppm; H-4, 5.19 ppm) were also assigned based on the reported assignment of hydrogens for pectin (Zhi et al., 2017). From the chemical shifts of anomeric protons, three sugars of GalA, Ara, and Rha adopted α-configuration (Wei et al., 2019). In contrast, TP exhibited stronger signal of GalA at 5.19 ppm, in agreement with the result that TP had higher content of GalA (longer HG).

3.1.3. Linkage analysis

To obtain the linkage patterns information, AP and TP were reduced and permethylated. Fig. S5 shows FT-IR spectra of the permethylated AP and TP. The stretching vibration bands of OH at 3600 ~ 3000 cm^{-1} almost disappeared, indicative of permethylation of all OH groups in AP and TP. The permethylated AP and TP were then used for hydrolysis, reduction, and acetylation, followed by GC-MS analysis. The sugar residues and their binding patterns are summarized in Table 2 according to the retention time of each peak in GC spectra and the fragment characteristics in MS patterns (Fig. S6-S8). It could be seen that AP and TP were mainly composed of GalA and Ara. In the case of AP, the molar ratios of Ara and GalA were estimated to be 38.2% and 39.9% respectively, in which Ara existed as (1 → 3)-, (1 → 5)-, and (1 → 2, 5)-linked furan ring residues (Ara*f*) as well as terminal residues (*T*-Ara*f*) with L-configuration. The (1 → 2, 3)-linked Ara existed as pyran ring residues, coded as Ara*p*. Of these, (1 → 5)-L-Ara*f* (16.9%) and *T*-L- Ara*f* (11.4%) occupied high proportions of all Ara sugar residues, revealing that RG-I region of AP was highly branched with Ara residues as terminals, similar to the reported pectin extracted from peach gum (Wei et al., 2019). The GalA residues with a pyran ring (GalA*p*) and D-configuration were linked by the α-1,4 linkages and accounted for the molar ratio of 35.6 % as the major linkage type. The (1 → 2, 4) bonding pattern of GalA*p* was also detected, indicating that C2 of (1 → 4)-linked GalA were branched,

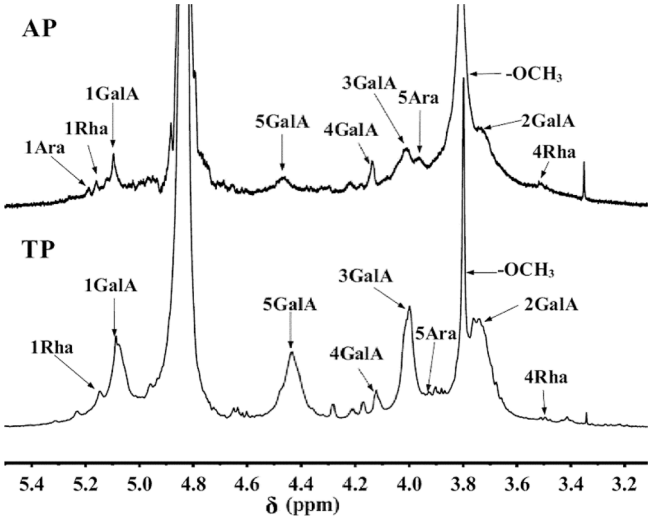

Fig. 2. The ^1H NMR spectra of AP and TP dissolved in D_2O with the concentration of 35 mg/mL (AP) and 50 mg/mL (TP), measured at 25 °C (the prefix numbers of monosaccharides are the order of carbon atoms linked with hydrogen atom in the sugar ring).

Table 2
Linkage patterns obtained from permethylated alditol acetates (PMAA) for AP and TP by GC-MS analysis (ND: not detected).

PMAA	Linkage patterns	Molar ratio (AP %)	Molar ratio (TP %)	Ion fragmentation (*m/z*)
2,3,5-Me_3-Ara	*T*-L-Ara*f*	11.4	3.2	71,87,102,118,129,161
2,5 -Me_2-Ara	1,3-L-Ara*f*	1.5	ND	87,99,118,129,160,233
2,3-Me_2-Ara	1,5-L-Ara*f*	16.9	11.6	87,102,118,129,189
4-Me-Ara	1,2,3-L-Ara*p*	5.5	9.7	85,99,118,127,159,261
3-Me-Ara	1,2,5-L-Ara*f*	2.9	2.7	87,118,129,146,189,207
3-Me-Rha	1,2,4-L-Rha*p*	2.9	ND	88,101,130,143,190,203
2,3,4,6-Me_4-Gal	*T*-D-GalA*p*	3.3	5.3	88,102,118,129,145,162,205
2,3,6-Me_3-Gal	1,4-D-GalA*p*	35.6	44.4	87,102,115,118,162,175,235
3,6-Me_2-Gal	1,2,4-D-GalA*p*	1.0	0.8	88,101,115,130,190,235
2,6-Me_2-Gal	1,3,4-D-Gal*p*	1.3	ND	87,117,129,143,185,231,305
2,4,6-Me_3-Gal	1,3-D-Gal*p*	0.9	ND	85,101,117,129,161,233,277
2,3,4-Me_3-Gal	1,6-D-Gal*p*	1.1	8.0	87,99,102,118,129,162,189
2,3-Me_2-Gal	1,4,6-D-Gal*p*	1.1	1.0	85,99,118,127,160,261
2,4-Me_2-Glc	1,3,6-D-Glc*p*	0.7	1.0	87,101,118,129,139,189,234
2,3-Me_2-Glc	1,4,6-D-Glc*p*	4.2	ND	85,101,117,127,256,261
unknown	unknown	9.7	12.4	—

which was ascribed to acetylation of GalA at C2. The molar ratio of (1,2,4)-GalA only accounted for 1%, further confirming the weak acetylation in FT-IR spectra. As reported, Rha was usually linked to GalA through (1 → 2)-Rha linkage in the backbone of RG-I region (Grassino et al., 2018). In our findings, Rha was detected as (1 → 2, 4)-L-Rha*p*, indicating that Rha was branched at C4, which was consistent with the reported pectin extracted from grapefruit peel (Wang et al., 2016) and Lonicera japonica Thunb (Liu et al., 2018). Gal and Glc residues were also multiple-branched with a pyran ring and D-configuration (Table 2).

As for TP, similar linkage patterns were identified, but these glycosidic bonds had different molar ratios. Excluding GalA (50.5%) as the major component, Ara was the second richest composition (27.2%) in TP. It was noted that the signals of some compounds in methylation analysis could not be summarized because of the trace amount.

3.2. Molecular weight and chain conformation

Molecular weight and molecular weight distribution were determined using SEC-MALLS at 30 °C. Fig. S9 shows SEC patterns and molecular weight distributions of the two pectin samples in 0.25 M $NaNO_3$ that completely inhibited the polyelectrolyte effect. The molecular weight value of AP changed from 3.0×10^4 to 9.0×10^5, and TP had a range of $5.0 \times 10^3 \sim 5.0 \times 10^4$. The statistical average values of M_w for AP and TP were calculated to be 243 kDa and 19 kDa (Table 3), respectively. Clearly, AP had much higher molecular weight than TP, confirming that molecular weight of pectin was strongly dependent on its source. Generally, natural polysaccharides have wide molecular weight distribution with $d > 2$ (Yang et al., 2018; Zhi et al., 2017). Interestingly, AP and TP exhibited a relatively low d value < 2, indicating that the two pectin samples had relatively narrow molecular weight distribution. It was worth noting that the R_z value of the flexible amylose in DMSO with a higher M_w of 344 kDa was determined to be

Table 3
The Intrinsic viscosity ([η]), weight-average molecular weights (M_w), z-average radii of gyration (R_z), and dispersity indices ($d \equiv M_w/M_n$) of the pectic polysaccharides.

Samples	[η] (dL/g)	$M_w \times 10^{-4}$	d (M_w/M_n)	R_z (nm)
AP	7.95 ± 0.02^a	24.3 ± 1.8^b	1.4 ± 0.03^b	51.2 ± 1.3^b
TP	0.53 ± 0.01^a	1.9 ± 0.2^b	1.8 ± 0.03^b	–

a, determined in 0.1 M $NaNO_3$ aqueous solution at 25 °C.
b, detected in 0.25 M $NaNO_3$ aqueous solution at 30 °C.

22.6 nm (Nakanishi, Norisuye, & Teramoto, 1993), much lower than the value of AP with lower M_w, suggesting that AP in aqueous solution adopted stiffer chain conformation than amylose in DMSO with flexible random coils. In principal, with common chain macromolecules of molecular weight lower than some $10^5 - 2 \times 10^5$ g/mol, no information on the particle size (let alone shape) can be obtained from light scattering; for macromolecules with molecular weights $2 \times 10^5 - 10^6$ g/mol, the radius of gyration can be measured with reasonable accuracy. Due to the much lower molecular weight of 1.9×10^4, the R_z of TP could not be accurately determined from light scattering.

Viscometry was used to further explore the chain conformation of AP and TP in aqueous solution. In general, the intrinsic viscosity reflects the hydrodynamic volume and chain stiffness of the polymer in solution (Ghimici, Nichifor, Eich, & Wolf, 2012). The macromolecular chains of pectin (as a polyelectrolyte) in protonated solvent should be relatively stretched due to the existence of electrostatic repulsion, leading to the sharp increase of viscosity with decreasing the concentration of polyelectrolyte (Li, Al-Assaf, Fang, & Phillips, 2013). Therefore, a non-linear dependence of viscosity on concentration occurs for the polyelectrolyte aqueous solution. Salts are usually used to screen the electrostatic repulsion of a polyelectrolyte in aqueous solution. Herein, $NaNO_3$ was used to shield the negative charges through interaction of Na^+ with COO^- on the pectin chains, and the effect of $NaNO_3$ concentration on [η] was thus studied.

As shown in Fig. 3A, a sharp decrease of [η] occurred with the increase in the concentration of $NaNO_3$. When the concentration of $NaNO_3$ was higher than 0.01 M, the [η] value leveled off, indicating that the electrostatic repulsion in AP aqueous solution was completely shielded. As for TP, the critical salt concentration that shielded the negative charges was determined to be 0.05 M (Fig. 3C) because of its higher GalA content and lower DM. After completely shielding electrostatic repulsion, the [η] values of AP and TP were determined to be 7.95 dL/g and 0.53 dL/g, respectively. Clearly, the [η] value of AP was much higher than that of TP, suggesting that AP had a bigger hydrodynamic volume than TP. The hydrodynamic volume of a polymer in solution depends on the two factors of molecular weight/chain length and charge density on the polymer chain. Herein, TP had more GalA and higher charge density than AP. Namely, TP had stronger electrostatic repulsion on the polysaccharide chain than AP, leading to the enhancement of hydrodynamic volume of TP. In combination, the bigger hydrodynamic volume of AP was mainly ascribed to its much higher M_w than TP. In combination of the data of M_w and R_z, the Flory viscosity factor Φ [$=[\eta]M_w/(6\ {R_z}^2)^{3/2}$] depending on chain stiffness was estimated to be 0.98×10^{23} $mol^{-1}$and 7.47×10^{20} $mol^{-1}$for AP and TP, respectively, indicating that AP was semi-flexible and TP was rigid within a limited molecular weight range (Norisuye, 1993).

As reported, the chain conformation of polyelectrolyte could be evaluated by an empirical method called '*B-value*' method according to the following equations (Smidsrød & Haug, 1971).

$$[\eta] = [\eta]_{0.1} + S(I^{-0.5} - 0.1^{-0.5}) \quad (6)$$

$$S = B[\eta]_{0.1}^{\rho} \quad (7)$$

where $[\eta]_{0.1}$ is the intrinsic viscosity (dL/g) at the ionic concentration of 0.1 M, ρ is a constant equal to 1.3 independent on polymer, and B is

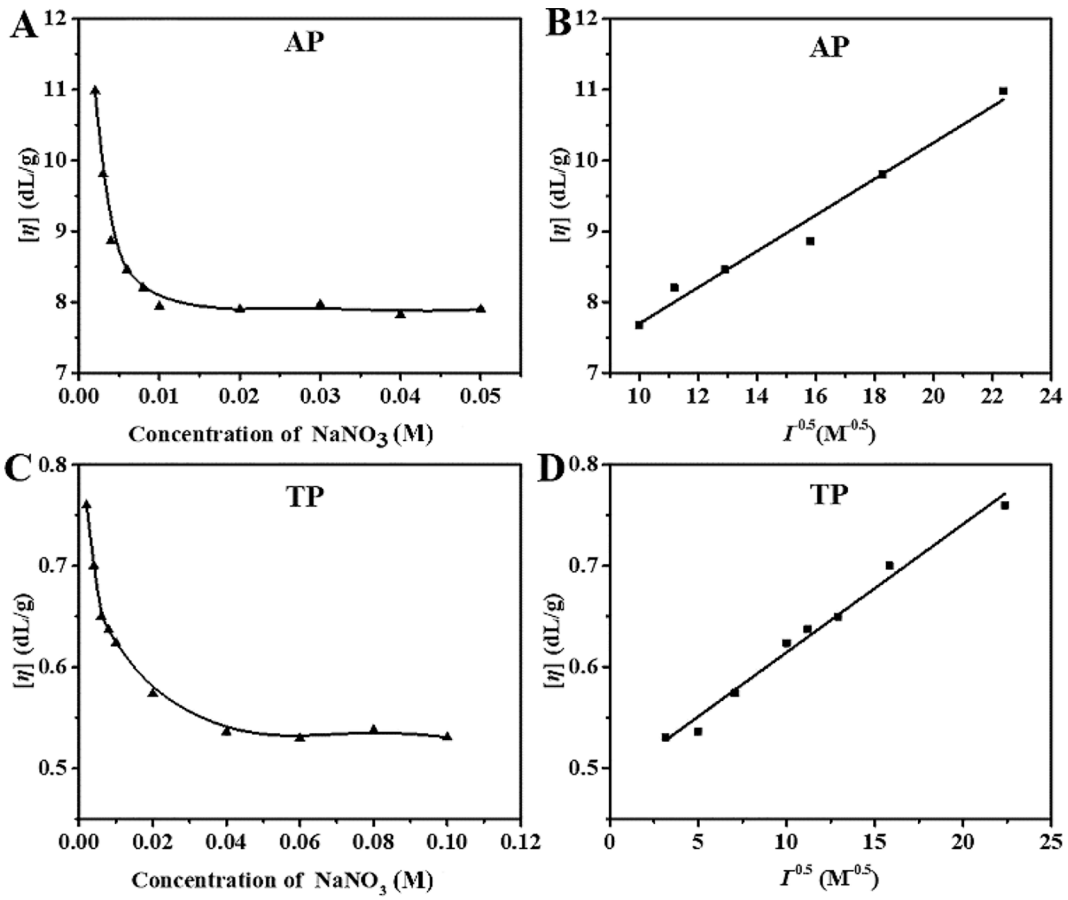

Fig. 3. Plots of intrinsic viscosity ([η]) versus concentration and ionic strength ($I^{-0.5}$) of $NaNO_3$ for AP (A, B) and TP (C, D) in water at 25 °C.

named as the '*B value*' depending on chain stiffness.

According to this method, the dependence of [η] on ionic strength ($I^{0.5}$) for the two pectin samples are shown in Fig. 3B and D. Apparently, [η] varied linearly with $I^{0.5}$, suggesting that the chain conformation of pectin polysaccharides could be determined by the *B-value* which was calculated from the slopes according to Eqs. 6 and 7. In our findings, the obtained *B-values* of AP (0.025) and TP (0.029) were significantly higher than that of the rigid xanthan gum (0.00525), much lower than that of flexible carboxymethyl amylose (0.2), and had the same order of magnitude as the semi-rigid carboxymethyl cellulose (0.043) or alginate (0.032) (Xu, Chen, Wang, & Zhang, 2009). These data indicated that both AP and TP adopt a semi-rigid chain conformation in $NaNO_3$ solution at 25 °C. The reason for the conformation of AP and TP might be that they have relatively stiff HG region and flexible neutral sugar side chains related to the content of galacturonic acid and rhamnose (Axelos & Thibault, 1991).

AFM is also a very convenient and appropriate tool for evaluating pectic molecules. Due to its high resolution, it is possible to image individual molecules or complexes in the natural environment, which cannot be achieved with any other method. In this study, to avoid the effect of $NaNO_3$, pectin samples were dissolved in pure water. As shown in Fig. 4A and B, both AP and TP dilute solutions with the concentration of 1.0 μg/mL after air-drying at room temperature existed as an extended shape. AP showed individual and bending chains ranging from 600 to 1600 nm in length and 0.4 – 1.0 nm in diameter, which was close to the pectin extracted from apple by Pieczywek et al. (2020). TP adopted individual rod-like morphology of chain lengths ranging from 200 to 400 nm with diameters in the range of 0.3 – 0.8 nm. These diameter values commensurate with the expected diameters of single polysaccharide strands when imaged by AFM (Round, Rigby, MacDougall, & Morris, 2010). The high molecular weight endowed AP relatively curly conformation, while the low molecular weight made TP rod-like stiff, similar to the water-soluble pectin extracted from fresh cherry tomatoes with short straight chains under AFM (Zhang, Wang, Sun, Chen, Lai, & Yang, 2020).

Taken together, AP and TP belonged to polyelectrolytes because of the presence of GalA, and showed strong electrostatic repulsion in water. TP adopted a higher-stiffness chain conformation in aqueous solution than AP due to the higher GalA content and lower molecular weight.

3.3. Aggregation morphology

To observe the macroscopic structure of pectic polysaccharides, SEM was performed. In this work, liquid nitrogen was used as the cryogen to quickly freeze the samples, and to minimize the effects of the formation of the ice crystals on the macroscopic structures. As shown in Fig. S10A-C, with a decrease of concentration of AP (1 mg/mL – 0.01 mg/mL), the macroscopic structure changed from irregular sheet to fibrous network. In contrast, TP showed less sheets and fibrous structure, which was ascribed to its lower molecular weight or shorter polysaccharide chains (Fig. S10D-F).

3.4. Steady-shear viscosity property and the correlation to chain conformation

Rheological behavior is very important to predict the quality of food and to guide the development of new products in the food industry (Lin, An, He, Geng, Song, & Huang, 2021). The rheological properties of polysaccharides are generally affected by its primary structure and conformation. Pectin exhibits more complex rheological behavior than neutral polysaccharides, because the addition of salt can change its chain conformation and interactions (Wee, Matia-Merino, & Goh, 2015).

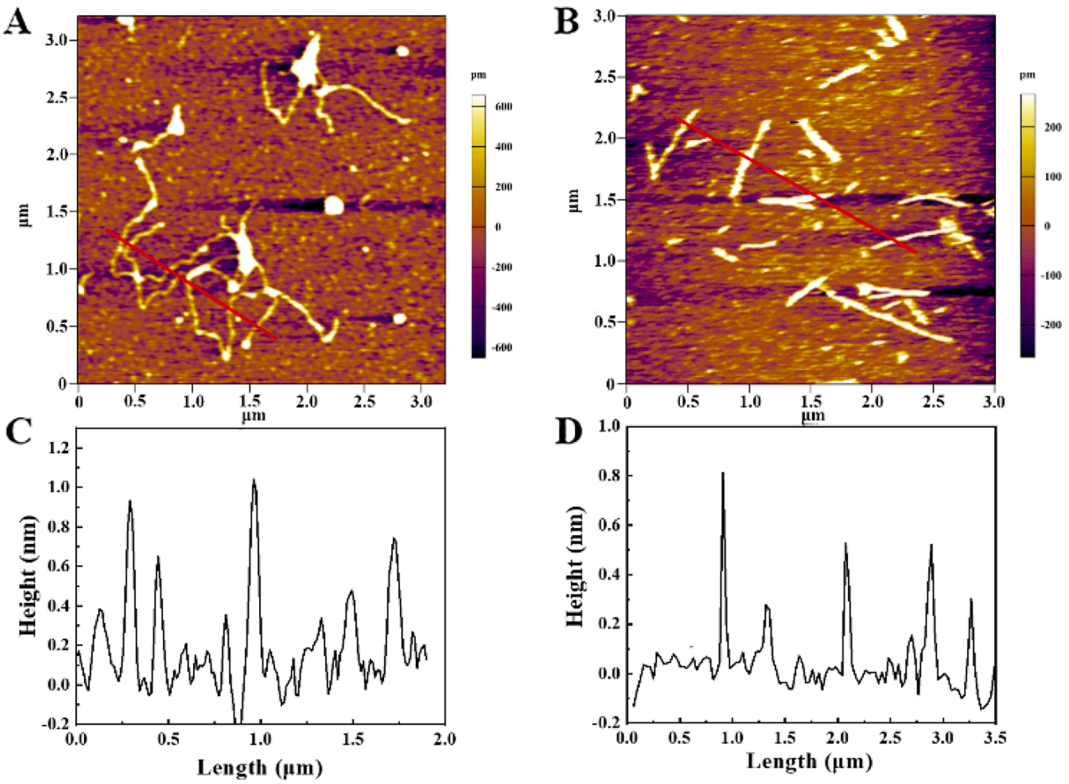

Fig. 4. AFM images of AP (A) and TP (B), and the heights of the indicated AP (C) and TP (D) chains by red lines in A and B. AP and TP were dissolved in water with a concentration of 1.0 μg/mL, followed by depositing on freshly cleaved mica and air-drying before observation. (For interpretation of the references to color in this figure legend, the reader is referred to the web version of this article.)

In this work, steady-shear rheological properties of pectin in water or $NaNO_3$ solutions with different concentrations were studied as shown in Fig. 5. The flow curves of AP and TP were fitted with the power law model in shear-thinning regions (Table S1). The bigger *k* and smaller *n* values reflect the stronger deviation from Newtonian flow behavior of a fluid. In our findings, the *k* values of AP and TP decreased with the increase of $NaNO_3$ concentration, but the effect of salt on *k* of AP (from 33.33 to 7.78) was greater than that of TP (from 6.56 to 4.34). In addition, the *n* values of AP increased from 0.24 to 0.49 with the increase of salt concentration, but it had little effect on that of TP (from 0.70 to 0.73). Obviously, AP solutions deviated from Newtonian flow behavior more strongly than TP. It was explained as AP had a higher molecular weight and a longer side chains linked to RG region than TP, leading to more chain entanglements formation and stronger shear thinning. In contrast, TP had a much lower molecular weight, leading to a weak shear-thinning flow with smaller *k* and bigger *n* values under the same conditions.

It was interesting that the Newtonian fluid flow in the low shear rate range of $< 1\ s^{-1}$ disappeared, but a shear-thickening behavior was observed, especially in the presence of $NaNO_3$. Subsequently, the shear-thinning behavior occurred with further increasing shear rate. To quantify the extent of shear thickening, we defined it as the ratio of peak viscosity during shear-thickening to the viscosity at onset of shear-thickening (η_{top}/η_{onset}). The index of η_{top}/η_{onset} increased with increasing $NaNO_3$ concentration for AP and TP (Table S1). As discussed in the section of molecular weight and chain conformation, AP and TP existed as extended semi-stiff conformation in $NaNO_3$ solution. The strong electrostatic repulsion of pectin chains in water was partially shielded by addition of $NaNO_3$, leading to increased interaction among macromolecular chains. The stiffness of AP and TP made them arrange with a certain degree of order at rest, leading to the small viscosity. Once a small shear (at low shear rate) was applied, the ordered arrangement was broken into randomly distributed entanglements, leading to the increased apparent viscosity. When the shear rate increased enough to break the entanglement, the chains would preferentially align along the shearing direction, leading to the regularly observed shear-thinning behavior. Therefore, the shear-thickening phenomenon in the low shear rate range was supposed to be attributed to the entanglement formation of pectin chains under shear stress due to the decreased electrostatic repulsion. Although similar phenomenon was observed in TP (Fig. 5B), it showed lower apparent viscosity and weaker shear-thickening property than AP. It could be explained as the lower molecular and shorter branches linked to RG region of TP led to less entanglements.

To test this conjecture, the steady-shear apparent viscosity of AP in pure water was simultaneously determined. As shown in Fig. 5C, the apparent viscosity increased with increasing AP concentrations within all the shear rate range, following the regular steady-shear viscosity properties of polymers. Of these, the Newtonian flow behavior was observed for AP at the concentration range of ≤ 15 mg/mL and the shear rate of below 1 s^{-1}. However, shear-thickening property was still observed at the low shear rate with increasing AP concentration from 20 to 30 mg/mL in water, although the extent of shear thickening was lower than that in $NaNO_3$ solutions. It indicated that the high concentration or the addition of salt ions increased interaction among chains due to the shielding of electrostatic repulsion, leading to more entanglement formation with stronger interaction in AP chains.

To confirm the interaction of pectin chains in the shear-thickening phenomenon, the steady-shear apparent viscosity of AP and TP in 0.1 M $NaNO_3$ solutions containing 4 M urea (a hydrogen bond breaking agent) was simultaneously determined. As a result, the decreased viscosity of AP and TP solutions after adding 4 M urea was clearly observed (Fig. 5D); at the same time, the shear thickening phenomenon also disappeared in the mixed solvent of 4 M urea and 0.1 M $NaNO_3$, demonstrating the interaction or entanglement of pectin chains were really disrupted to eliminate the shear thickening phenomenon under

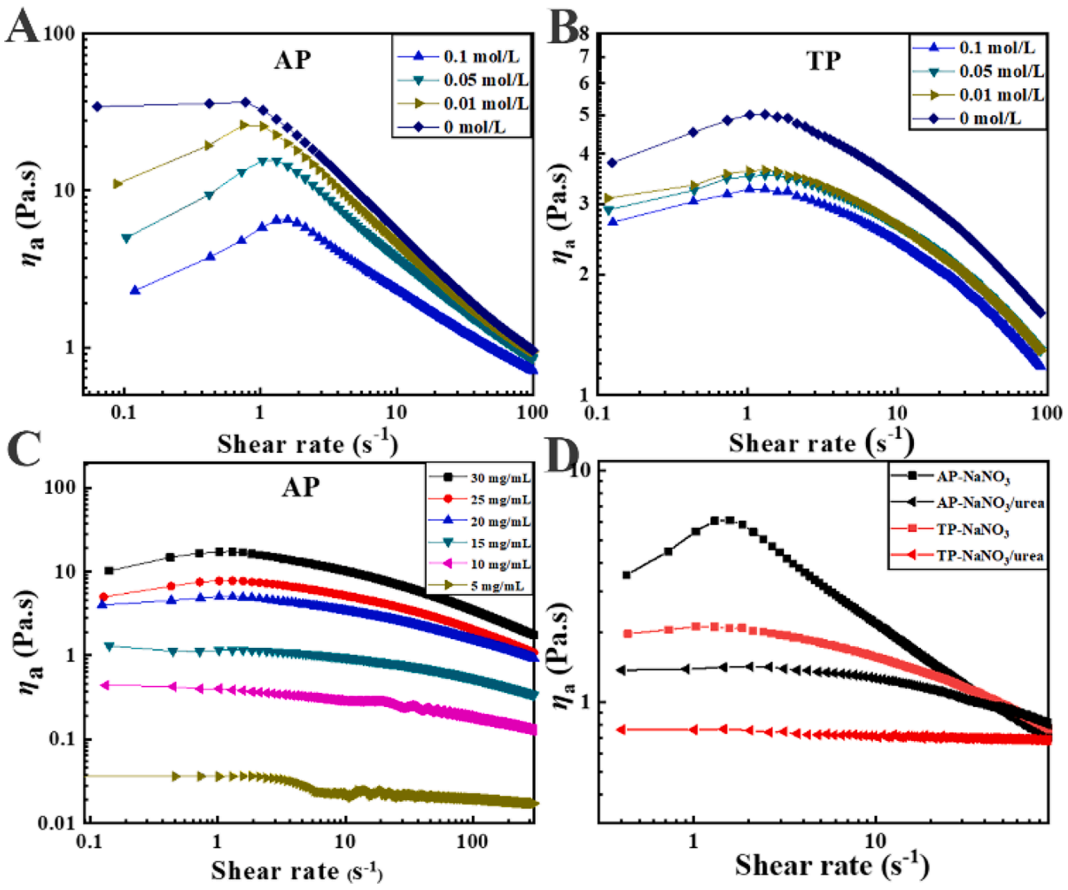

Fig. 5. The shear rate dependence of apparent viscosity η_a for samples AP (A) and TP (B) in water (20 mg/mL) with the $NaNO_3$ concentration of 0–0.1 M at 25 °C, and different concentrations of AP (5 m g/mL- 30 mg/mL) in water (C). The shear rate dependence of η_a in 0.1 M $NaNO_3$ solution or the mixed solution of 4 M urea and 0.1 M $NaNO_3$ (D).

low shear.

From the Newtonian platform, the zero-shear viscosities (η_0) of AP and TP in water with different concentrations were estimated, and the concentration dependence of η_0 is shown in Fig. S11. η_0 changed non-linearly with concentration as scaled as $\eta_0 \propto c^{3.89}$ for AP, and $\eta_0 \propto c^{2.32}$ for TP, suggesting that AP and TP were in the concentrated regime to form an entangled network with the bigger exponent than 1 (Xu, Xu, Zhang, & Zhang, 2008). This result further confirmed the entanglement formation for AP and TP in aqueous solution.

4. Conclusions

In this work, two pectic polysaccharides were respectively extracted from apples and tomatoes. Apple pectin was identified to be a high-ester pectin with a short HG region and the long neutral sugar side chain. Tomato pectin was a low-ester pectin with a long HG region and short neutral sugar side chain. The weight-average molecular weights for apple pectin and tomato pectin were determined to be 243 kDa and 19 kDa, respectively, indicating a strong dependence of sources on molecular weight. Two pectic polysaccharides adopted a semi-rigid conformation according to the empirical method of Smidsrød '*B-value*' for polyelectrolytes in water containing $NaNO_3$. Of these, TP adopted a higher-stiffness chain conformation due to the higher GalA content and lower molecular weight, which was visually confirmed by AFM images. Both of AP and TP with the high concentration showed shear-thinning behavior at high shear rate, and shear-thickening behavior at low shear rate due to the strong chain entanglement effect resulted from the high molecular weight and strong interaction of pectin chains. These findings provide important information for controlling the viscosity of pectic polysaccharides containing salt during food processing.

CRediT authorship contribution statement

Shihao Hu: Conceptualization, Methodology, Software, Data curation, Writing – original draft, Visualization, Investigation. **Junqiao Wang:** Methodology, Software, Data curation. **Shaoping Nie:** Supervision, Validation. **Qiang Wang:** Funding acquisition, Project administration, Supervision, Validation. **Xiaojuan Xu:** Conceptualization, Funding acquisition, Project administration, Methodology, Supervision, Validation, Writing – review & editing.

Declaration of Competing Interest

The authors declare that they have no known competing financial interests or personal relationships that could have appeared to influence the work reported in this paper.

Acknowledgements

We gratefully acknowledge the financial supports from the National Key Research and Development Plan (2016YFD0400202), National Natural Science Foundation of China (22075213, 21875167, and 21574102), and Key Research and Development Program of Hubei Province (2020BCA079).

Appendix A. Supplementary data

Supplementary data to this article can be found online at https://doi.

org/10.1016/j.fochx.2022.100296.

References

Axelos, M. A. V., & Thibauit, J.-F. (1991). Influence of the substituents of the carboxyl groups and of the rhamnose content on the solution properties and flexibility of pectins. *International Journal of Biological Macromolecules, 2*(13), 77–82. https://doi.org/10.1016/0141-8130(91)90052-V

Barreira, J. C. M., Arraibi, A. A., & Ferreira, I. C. F. R. (2019). Bioactive and functional compounds in apple pomace from juice and cider manufacturing: Potential use in dermal formulations. *Trends in Food Science & Technology, 90*, 76–87. https://doi.org/10.1016/j.tifs.2019.05.014

Cao, L., Lu, W., Mata, A., Nishinari, K., & Fang, Y. (2020). Egg-box model-based gelation of alginate and pectin: A review. *Carbohydrate Polymers, 242*, 116389. https://doi.org/10.1016/j.carbpol.2020.116389

Celus, M., Kyomugasho, C., Van Loey, A. M., Grauwet, T., & Hendrickx, M. E. (2018). Influence of Pectin Structural Properties on Interactions with Divalent Cations and Its Associated Functionalities. *Comprehensive Reviews In Food Science And Food Safety, 17*(6), 1576–1594. https://doi.org/10.1111/1541-4337.12394

Cheng, Y., Xie, Y., Ge, J. C., Wang, L., Peng, D. Y., Yu, N. J., & Chen, W. D. (2021). Structural characterization and hepatoprotective activity of a galactoglucan from Poria cocos. *Carbohydrate Polymers, 263*, 117979. https://doi.org/10.1016/j.carbpol.2021.117979

Ciucanu, I., & Kerek, F. (1984). A simple and rapid method for the permethylation of carbohydrates. *Carbohydrate Research, 131*(2), 209–217. 10.1016/0008-6215(84)85242-8.

Colodel, C., Vriesmann, L. C., Teofilo, R. F., & de Oliveira Petkowicz, C. L. (2018). Extraction of pectin from ponkan (Citrus reticulata Blanco cv. Ponkan) peel: Optimization and structural characterization. *International Journal of Biological Macromolecules, 117*, 385–391. https://doi.org/10.1016/j.ijbiomac.2018.05.048

Cui, J., Zhao, C., Feng, L., Han, Y., Du, H., Xiao, H., & Zheng, J. (2021). Pectins from fruits: Relationships between extraction methods, structural characteristics, and functional properties. *Trends in Food Science & Technology, 110*, 39–54. https://doi.org/10.1016/j.tifs.2021.01.077

Dranca, F., & Oroian, M. (2018). Extraction, purification and characterization of pectin from alternative sources with potential technological applications. *Food Research International, 113*, 327–350. https://doi.org/10.1016/j.foodres.2018.06.065

Ghimici, L., Nichifor, M., Eich, A., & Wolf, B. A. (2012). Intrinsic viscosities of polyelectrolytes in the absence and in the presence of extra salt: Consequences of the stepwise conversion of dextran into a polycation. *Carbohydrate Polymers, 87*(1), 405–410. https://doi.org/10.1016/j.carbpol.2011.07.067

Grassino, A. N., Brncic, M., Vikic-Topic, D., Roca, S., Dent, M., & Brncic, S. R. (2016). Ultrasound assisted extraction and characterization of pectin from tomato waste. *Food Chemistry, 198*, 93–100. https://doi.org/10.1016/j.foodchem.2015.11.095

Grassino, A. N., Halambek, J., Djaković, S., Rimac Brnčić, S., Dent, M., & Grabarić, Z. (2016). Utilization of tomato peel waste from canning factory as a potential source for pectin production and application as tin corrosion inhibitor. *Food Hydrocolloids, 52*, 265–274. https://doi.org/10.1016/j.foodhyd.2015.06.020

Grassino, A. N., Barba, F. J., Brncic, M., Lorenzo, J. M., Lucini, L., & Brncic, S. R. (2018). Analytical tools used for the identification and quantification of pectin extracted from plant food matrices, wastes and by-products: A review. *Food Chemistry, 266*, 47–55. https://doi.org/10.1016/j.foodchem.2018.05.105

He, F., Zhang, S., Li, Y., Chen, X., Du, Z., Shao, C., & Ding, K. (2021). The structure elucidation of novel arabinogalactan LRP1-S2 against pancreatic cancer cells growth in vitro and in vivo. *Carbohydrate Polymers, 267*, 118172. https://doi.org/10.1016/j.carbpol.2021.118172

Huggins, M. L. (1942). The viscosity of dilute solutions of long-chain molecules. IV. Dependence on concentration. *Journal of the American Chemical Society, 64*, 2716–2718. https://doi.org/10.1021/ja01263a056

Humerez-Flores, J. N., Kyomugasho, C., Gutierrez-Ortiz, A. A., De Bie, M., Panozzo, A., Van Loey, A. M., & Hendrickx, M. E. (2022). Production and molecular characterization of tailored citrus pectin-derived compounds. *Food Chemistry, 367*, 130635. https://doi.org/10.1016/j.foodchem.2021.130635

Kermani, Z. J., Shpigelman, A., Kyomugasho, C., Buggenhout, S. V., Ramezani, M., Van Loey, A. M., & Hendrickx, M. E. (2014). The impact of extraction with a chelating agent under acidic conditions on the cell wall polymers of mango peel. *Food Chemistry, 161*, 199–207. https://doi.org/10.1016/j.foodchem.2014.03.131

Kjøniksen, A.-L., Hiorth, M., & Nyström, B. (2005). Association under shear flow in aqueous solutions of pectin. *European Polymer Journal, 41*(4), 761–770. https://doi.org/10.1016/j.eurpolymj.2004.11.006

Kyomugasho, C., Christiaens, S., Shpigelman, A., Van Loey, A. M., & Hendrickx, M. E. (2015). FT-IR spectroscopy, a reliable method for routine analysis of the degree of methylesterification of pectin in different fruit- and vegetable-based matrices. *Food Chemistry, 176*, 82–90. https://doi.org/10.1016/j.foodchem.2014.12.033

Li, X., Al-Assaf, S., Fang, Y., & Phillips, G. O. (2013). Characterisation of commercial LM-pectin in aqueous solution. *Carbohydrate Polymers, 92*(2), 1133–1142. https://doi.org/10.1016/j.carbpol.2012.09.100

Lin, Y., An, F., He, H., Geng, F., Song, H., & Huang, Q. (2021). Structural and rheological characterization of pectin from passion fruit (Passiflora edulis f. flavicarpa) peel extracted by high-speed shearing. *Food Hydrocolloids, 114*. https://doi.org/10.1016/j.foodhyd.2020.106555

Liu, Q., Fang, J., Wang, P., Du, Z., Li, Y., Wang, S., & Ding, K. (2018). Characterization of a pectin from Lonicera japonica Thunb. and its inhibition effect on Abeta42 aggregation and promotion of neuritogenesis. *International Journal of Biological Macromolecules, 107*(Pt A), 112-120. https://doi.org/10.1016/j.ijbiomac.2017.08.154.

Ma, J. S., Liu, H., Han, C. R., Zeng, S. J., Xu, X. J., Lu, D. J., & He, H. J. (2020). Extraction, characterization and antioxidant activity of polysaccharide from Pouteria campechiana seed. *Carbohydrate Polymers, 229*, 115409. https://doi.org/10.1016/j.carbpol.2019.115409

Marić, M., Grassino, A. N., Zhu, Z., Barba, F. J., Brnčić, M., & Rimac Brnčić, S. (2018). An overview of the traditional and innovative approaches for pectin extraction from plant food wastes and by-products: Ultrasound-, microwaves-, and enzyme-assisted extraction. *Trends in Food Science & Technology, 76*, 28–37. https://doi.org/10.1016/j.tifs.2018.03.022

Mendez, D. A., Fabra, M. J., Gomez-Mascaraque, L., Lopez-Rubio, A., & Martinez-Abad, A. (2021). Modelling the Extraction of Pectin towards the Valorisation of Watermelon Rind Waste. *Foods, 10*(4). https://doi.org/10.3390/foods10040738

Morris, G. A., de al Torre, J. G., Ortega, A., Castile, J., Smith, A., & Harding, S. E. (2008). Molecular flexibility of citrus pectins by combined sedimentation and viscosity analysis. *Food Hydrocolloids, 22*(8), 1435–1442. 10.1016/j.foodhyd.2007.09.005.

Moslemi, M. (2021). Reviewing the recent advances in application of pectin for technical and health promotion purposes: From laboratory to market. *Carbohydrate Polymers, 254*, 117324. https://doi.org/10.1016/j.carbpol.2020.117324

Muhammad, K., Mohd. Zahari, N. I., Gannasin, S. P., Mohd. Adzahan, N., & Bakar, J. (2014). High methoxyl pectin from dragon fruit (Hylocereus polyrhizus) peel. *Food Hydrocolloids, 42*, 289–297. 10.1016/j.foodhyd.2014.03.021.

Munoz-Almagro, N., Montilla, A., & Villamiel, M. (2021). Role of pectin in the current trends towards low-glycaemic food consumption. *Food Research International, 140*, 109851. https://doi.org/10.1016/j.foodres.2020.109851

Nakanishi, Y., Norisuye, T., & Teramoto, A. (1993). Conformation of Amylose in Dimethyl Sulfoxide. *Macromolecules, 26*(16), 4220–4225. https://doi.org/10.1021/ma00068a023

Neckebroeck, B., Verkempinck, S. H. E., Van Audenhove, J., Bernaerts, T., de Wilde d'Estmael, H., Hendrickx, M. E., & Van Loey, A. M. (2021). Structural and emulsion stabilizing properties of pectin rich extracts obtained from different botanical sources. *Food Research International, 141*, 110087. https://doi.org/10.1016/j.foodres.2020.110087

Norisuye, T. (1993). Semiflexible polymers in dilute solution. *Progress in Polymer Science, 18*(3), 543–584. https://doi.org/10.1016/0079-6700(93)90017-7

Petkowicz, C. L. O., Vriesmann, L. C., & Williams, P. A. (2017). Pectins from food waste: Extraction, characterization and properties of watermelon rind pectin. *Food Hydrocolloids, 65*, 57–67. https://doi.org/10.1016/j.foodhyd.2016.10.040

Pieczywek, P. M., Kozioł, A., Płaziński, W., Cybulska, J., & Zdunek, A. (2020). Resolving the nanostructure of sodium carbonate extracted pectins (DASP) from apple cell walls with atomic force microscopy and molecular dynamics. *Food Hydrocolloids, 104*. https://doi.org/10.1016/j.foodhyd.2020.105726

Purnomo, E. H., Sitanggang, A. B., & Nabilah, U. U. (2021). Rheological method for determination of critical concentration of pectin dispersion – A review. *The Annals of the University Dunarea de Jos of Galati Fascicle VI – Food Technology, 45*(2), 180–202. 10.35219/foodtechnology.2021.2.12.

Reichembach, L. H., & Lúcia de Oliveira Petkowicz, C. (2021). Pectins from alternative sources and uses beyond sweets and jellies: An overview. *Food Hydrocolloids, 118*. 10.1016/j.foodhyd.2021.106824.

Round, A. N., Rigby, N. M., MacDougall, A. J., & Morris, V. J. (2010). A new view of pectin structure revealed by acid hydrolysis and atomic force microscopy. *Carbohydrate Research, 345*(4), 487–497. https://doi.org/10.1016/j.carres.2009.12.019

Sengar, A. S., Rawson, A., Muthiah, M., & Kalakandan, S. K. (2020). Comparison of different ultrasound assisted extraction techniques for pectin from tomato processing waste. *Ultrasonics Sonochemistry, 61*, 104812. https://doi.org/10.1016/j.ultsonch.2019.104812

Shen, C., Wang, T., Guo, F., Sun, K., Wang, B., Wang, J., & Chen, Y. (2021). Structural characterization and intestinal protection activity of polysaccharides from Sea buckthorn (Hippophae rhamnoides L.) berries. *Carbohydrate Polymers, 274*, 118648. https://doi.org/10.1016/j.carbpol.2021.118648

Shivamathi, C. S., Gunaseelan, S., Soosai, M. R., Vignesh, N. S., Varalakshmi, P., Kumar, R. S., & Ganesh Moorthy, I. M. (2022). Process optimization and characterization of pectin derived from underexploited pineapple peel biowaste as a value-added product. *Food Hydrocolloids, 123*. https://doi.org/10.1016/j.foodhyd.2021.107141

Smidsrød, O., & Haug, A. (1971). Estimation of the relative stiffness of the molecular chain in polyelectrolytes from measurements of viscosity at different ionic strengths. *Biopolymers: Original Research on Biomolecules, 10*(7), 1213–1227. https://doi.org/10.1002/bip.360100711

Surenjav, U., Zhang, L., Xu, X., Zhang, X., & Zeng, F. (2006). Effects of molecular structure on antitumor activities of (1→3)-β-D-glucans from different Lentinus edodes. *Carbohydrate Polymers, 63*(1), 97–104. https://doi.org/10.1016/j.carbpol.2005.08.011

Tang, W., Liu, D., Wang, J. Q., Huang, X. J., Yin, J. Y., Geng, F., & Nie, S. P. (2021). Isolation and structure characterization of a low methyl-esterified pectin from the tuber of Dioscorea opposita Thunb. *Food Chemistry, 359*, 129899. https://doi.org/10.1016/j.foodchem.2021.129899

Taylor, R. L., & Conrad, H. E. (1972). Stoichiometric depolymerization of polyuronides and glycosaminoglycuronans to monosaccharides following reduction of their carbodiimide-activated carboxyl group. *Biochemistry, 11*(8), 1383–1388. https://doi.org/10.1021/bi00758a009

Voragen, A.G.J., Schols, H.A., & Pilnik, W. (1986). Determination of the degree of methylation and acetylation of pectins by h.p.l.c,. *Food Hydrocolloids, 1*(1), 65–70. 10.1016/S0268-005X(86)80008-X.

Wang, W., Ma, X., Jiang, P., Hu, L., Zhi, Z., Chen, J., & Liu, D. (2016). Characterization of pectin from grapefruit peel: A comparison of ultrasound-assisted and conventional heating extractions. *Food Hydrocolloids, 61*, 730–739. https://doi.org/10.1016/j.foodhyd.2016.06.019

Wee, M. S., Matia-Merino, L., & Goh, K. K. (2015). The cation-controlled and hydrogen bond-mediated shear-thickening behaviour of a tree-fern isolated polysaccharide. *Carbohydrate Polymers, 130*, 57–68. https://doi.org/10.1016/j.carbpol.2015.03.086

Wei, C., Zhang, Y., He, L., Cheng, J., Li, J., Tao, W., … Chen, S. (2019). Structural characterization and anti-proliferative activities of partially degraded polysaccharides from peach gum. *Carbohydrate Polymers, 203*, 193–202. https://doi.org/10.1016/j.carbpol.2018.09.029

Xiong, B., Zhang, W., Wu, Z., Liu, R., Yang, C., Hui, A., & Xian, Z. (2021). Preparation, characterization, antioxidant and anti-inflammatory activities of acid-soluble pectin from okra (Abelmoschus esculentus L.). *International Journal of Biological Macromolecules, 181*, 824–834. https://doi.org/10.1016/j.ijbiomac.2021.03.202

Xu, X., Xu, J., Zhang, Y., & Zhang, L. (2008). Rheology of triple helical Lentinan in solution: Steady shear viscosity and dynamic oscillatory behavior. *Food Hydrocolloids, 22*(5), 735–741. https://doi.org/10.1016/j.foodhyd.2007.02.010

Xu, X., Chen, P., Wang, Y., & Zhang, L. (2009). Chain conformation and rheological behavior of an extracellular heteropolysaccharide Erwinia gum in aqueous solution. *Carbohydrate Research, 344*(1), 113–119. https://doi.org/10.1016/j.carres.2008.10.009

Xu, X., Zhang, L., Yagoub, A. E. A., Yu, X., Ma, H., & Zhou, C. (2021). Effects of ultrasound, freeze-thaw pretreatments and drying methods on structure and functional properties of pectin during the processing of okra. *Food Hydrocolloids, 120*. https://doi.org/10.1016/j.foodhyd.2021.106965

Yang, J. S., Mu, T. H., & Ma, M. M. (2018). Extraction, structure, and emulsifying properties of pectin from potato pulp. *Food Chemistry, 244*, 197–205. https://doi.org/10.1016/j.foodchem.2017.10.059

Zdunek, A., Pieczywek, P. M., & Cybulska, J. (2021). The primary, secondary, and structures of higher levels of pectin polysaccharides. *Comprehensive Reviews in Food Science and Food Safety, 20*(1), 1101–1117. https://doi.org/10.1111/1541-4337.12689

Zhang, L., Wang, P., Sun, X., Chen, F., Lai, S., & Yang, H. (2020). Calcium permeation property and firmness change of cherry tomatoes under ultrasound combined with calcium lactate treatment. *Ultrasonics Sonochemistry, 60*, 104784. https://doi.org/10.1016/j.ultsonch.2019.104784

Zhang, W., Xie, F., Liu, X., Luo, J., Wu, J., & Wang, Z. (2019). Pectin from Black Tomato Pomace: Characterization, Interaction with Gallotannin, and Emulsifying Stability Properties. *Starch-Stärke, 71*, 1800172. https://doi.org/10.1002/star.201800172

Zheng, X., Lu, F., Xu, X., & Zhang, L. (2017). Extended chain conformation of β-glucan and its effect on antitumor activity. *Journal of Materials Chemistry B, 5*(28), 5623–5631. https://doi.org/10.1039/C7TB01324H

Zheng, J., Li, H., Wang, D., Li, R., Wang, S., & Ling, B. (2021). Radio frequency assisted extraction of pectin from apple pomace: Process optimization and comparison with microwave and conventional methods. *Food Hydrocolloids, 121*. https://doi.org/10.1016/j.foodhyd.2021.107031

Zhi, Z., Chen, J., Li, S., Wang, W., Huang, R., Liu, D., & Ye, X. (2017). Fast preparation of RG-I enriched ultra-low molecular weight pectin by an ultrasound accelerated Fenton process. *Scientific Reports, 7*(1), 541. https://doi.org/10.1038/s41598-017-00572-3

Zhu, M., Huang, R., Wen, P., Song, Y., He, B., Tan, J., & Wang, H. (2021). Structural characterization and immunological activity of pectin polysaccharide from kiwano (Cucumis metuliferus) peels. *Carbohydrate Polymers, 254*, 117371. https://doi.org/10.1016/j.carbpol.2020.117371

Ziari, H., Ashtiani, F. Z., & Mohtashamy, M. (2010). Comparing the effectiveness of processing parameters in pectin extraction from apple pomace. *Afinidad, 67*, 6. https://doi.org/10.1016/j.jpcs.2010.04.018